Energy & Environmental Science

Cite this: *Energy Environ. Sci.*, 2011, **4**, 2922

www.rsc.org/ees



**PAPER**

# Enhancement of photocurrent and photocatalytic activity of ZnO hybridized with graphite-like $C_3N_4$†

**Yajun Wang, Rui Shi, Jie Lin and Yongfa Zhu***

***Received 27th December 2010, Accepted 20th April 2011***
**DOI: 10.1039/c0ee00825g**



A ZnO photocatalyst was hybridized with graphite-like $C_3N_4$ *via* a monolayer-dispersed method. After hybridization with $C_3N_4$, the photocurrent of ZnO was enhanced by 5 times under UV irradiation and a photocurrent under visible light irradiation was observed. The photocatalytic activity of $C_3N_4$/ZnO under UV irradiation was increased by 3.5 times, the visible light photocatalytic activity was generated and the photocorrosion of ZnO was suppressed completely after ZnO was hybridized with $C_3N_4$. The enhancement in performance and photocorrosion inhibition under UV irradiation was induced by the high separation efficiency of photoinduced holes from ZnO to the HOMO of $C_3N_4$. Under visible light irradiation, the electron excited from the HOMO to the LUMO of $C_3N_4$ could directly inject into the CB of ZnO, making $C_3N_4$/ZnO present visible light photocatalytic activity. The optimum synergetic effect of $C_3N_4$/ZnO was found at a weight ratio of 3%, which corresponded to a monolayer dispersion of $C_3N_4$ on the surface of ZnO.

## Introduction

In recent years, photocatalysis has attracted much attention in water treatment due to its total destruction ability of pollutants and broad compound applicability.[1] Among various semiconductor materials in present research, although $TiO_2$ has been extensively investigated and widely employed, ZnO appears to be a suitable alternative to $TiO_2$. ZnO is also relatively inexpensive and its photodegradation mechanism is similar to that of $TiO_2$.[2,3] Moreover, some studies have highlighted that ZnO exhibits a higher efficiency than $TiO_2$ in the photocatalytic degradation of some dyes in water and photoelectric conversion.[4–7] However, the high recombination ratio of photoinduced electron–hole pairs, very poor response to visible light and the photocorrosion have hindered the application of ZnO in photocatalysis. Some effort has been devoted to reducing the recombination of photogenerated electron–hole pairs and improving the utilization of solar light of ZnO, such as doping,[8,9] deposition of metals,[10–12] or combining ZnO with another semiconductor.[13,14] It is anticipated that ZnO could become an excellent photocatalyst if the photocorrosion can be suppressed. However, few reports have focused on this topic. It has been reported by He and co-workers that a ZnO/reduced graphite oxide composite exhibited higher photocatalytic activity and a photocorrosion improvement.[15] Comparelli and co-workers found that surface organic coating of ZnO could provide the oxide with photocorrosion resistance and pH variation.[16]

Materials with delocalized conjugated π structures have been extensively studied in electron-transfer processes due to their rapid photoinduced charge separation and a relatively slow charge recombination.[17] A delocalized conjugated π structure material combined with a semiconductor may act as a novel "dyade" type structure which could form a common conjugated

*Department of Chemistry, Tsinghua University, Beijing, 100084, China. E-mail: zhuyf@mail.tsinghua.edu.cn; Fax: +86-10-62787601; Tel: +86-10-62787601*

† Electronic supplementary information (ESI) available. See DOI: 10.1039/c0ee00825g

### Broader context

Semiconductor photocatalysis has attracted considerable attention since it has great potential in environmental remediation and hydrogen energy production. Although $TiO_2$ has been extensively investigated and widely employed, ZnO appears to be a suitable alternative to $TiO_2$. ZnO is also relatively inexpensive and its photodegradation mechanism is similar to that of $TiO_2$. But the photocorrosion, the high recombination ratio of photoinduced electron–hole pairs and very poor response to visible light have hindered the application of ZnO in photocatalysis. This article reports the first example of a $C_3N_4$-hybridized ZnO photocatalyst to enhance the photocatalytic activity and suppress the photocorrosion. The as-prepared $C_3N_4$-hybridized ZnO possesses significantly enhanced UV light photocatalytic activity, visible light photocatalytic activity and excellent antiphotocorrosion ability.

system and improve the photocatalytic activity in the complete spectral range.[18,19] Our group has developed conjugative π structure material hybridized ZnO as efficient photocatalysts and successfully suppressed the photocorrosion, for example using $C_{60}$,[20] polyaniline,[21] and graphite.[22] Graphite-like $C_3N_4$ (denoted as $C_3N_4$) is the most stable material of all the carbon nitride allotropes under ambient conditions.[23] $C_3N_4$ possesses a very high thermal and chemical stability; it has attracted a great deal of scientific interest due to its outstanding mechanical, electrical, thermal, and optical properties.[24] Some studies have focused on the applications of $C_3N_4$ materials in photo-splitting water[25–30] and organic pollutant degradation.[31,32] Some effort has been devoted to enhancing the photocatalytic activity of $C_3N_4$, such as by dye-sensitization,[26] transition metal-modification,[29] and combination of $C_3N_4$ with a metal to form heterojunctions.[30]

$C_3N_4$ has a conjugated π structure and the combination of ZnO and $C_3N_4$ may be an ideal system to achieve an enhanced charge separation in electron-transfer processes and suppress the photocorrosion. To the best of our knowledge, there has been no report regarding the introduction of $C_3N_4$ to ZnO to enhance the photocatalytic activity and suppress the photocorrosion. Herein, we present the first example of a $C_3N_4$-hybridized ZnO photocatalyst fabricated by the chemisorption method and demonstrate that a hybrid effect exists between ZnO and $C_3N_4$. The photoelectrochemical performances and methylene blue (MB) degradation performance were investigated systematically. After hybridization with $C_3N_4$, the photocurrent of ZnO was enhanced by 5 times under UV irradiation and a photocurrent under visible light irradiation was observed. The degradation results indicated that the introduction of $C_3N_4$ to ZnO can effectively enhance the UV light photocatalytic activity, generate visible photocatalytic activity, and suppress the photocorrosion. The synergic effect between ZnO and $C_3N_4$, the possible mechanisms of photocorrosion inhibition and enhancement of photocatalytic activity *via* hybridization were also investigated.

## Experimental section

### Preparation of the $C_3N_4$/ZnO photocatalyst

Melamine ($C_3H_6N_6$) was purchased from Sinopharm Chemical Reagent Corp, P. R. China; ZnO (particle diameter 20 nm, surface area 37.741 $m^2\ g^{-1}$) was obtained from Nanjing Haitai Nanometer Materials Corp, P. R. China. All other reagents used in this research were analytically pure and used without further purification. The $C_3N_4$ used in this study was prepared by heating melamine to 550 °C for 2 h in $N_2$ atmosphere according to the literature.[25] The typical preparation of $C_3N_4$/ZnO photocatalysts was as follows: firstly, an appropriate amount of $C_3N_4$ was added into methanol then the beaker was placed in an ultrasonic bath for 30 min to completely disperse the $C_3N_4$. The ZnO powder was added into the above solution and stirred in a fume hood for 24 h. After volatilization of the methanol, an opaque powder was obtained after drying at 100 °C in $N_2$ atmosphere. According to this method, different mass ratios of $C_3N_4$/ZnO photocatalysts from 1% to 8% were synthesized.

To investigate the transition of photogenerated electrons before and after $C_3N_4$ hybridization, ZnO and $C_3N_4$/ZnO electrodes were prepared as follows: 5 mg of the as-prepared photocatalyst was suspended in 5 mL ethanol to produce a slurry, which was then dip-coated onto a 2 cm × 4 cm indium-tin oxide (ITO) glass electrode. Electrodes were exposed to UV light for 12 h to eliminate ethanol and subsequently calcined at 200 °C for 30 min under $N_2$ flow (rate = 60 mL $min^{-1}$). All investigated electrodes were of similar thickness (0.8–1.0 μm).

### Characterization

Fourier transform infrared (FT-IR) spectra were measured by a Perkin Elmer System 2000 infrared spectrometer with KBr as the reference sample. The morphologies and structure of the as-prepared samples were examined with transmission electron microscopy (TEM) by a JEM 1010 electron microscope operated at an accelerating voltage of 100 kV. The high-resolution transmission electron microscopy (HRTEM) images were obtained by Tecnai TF20 transmission electron microscope operated at an accelerating voltage of 200 kV. UV-Vis diffuse reflectance spectroscopy (DRS) was carried out on a Hitachi U-3010 UV-vis spectrophotometer. $BaSO_4$ was the reference sample. The Brunauer-Emmett-Teller (BET) surface area was measured by ASAP 2010 V5.02H. The crystallinity of the as-prepared sample was characterized by X-ray diffraction (XRD) on Bruker D8-advance diffractometer using Cu-Kα radiation (λ = 1.5418 Å). Thermogravimetric analysis (TG) was performed in air at a heating rate of 10 °C $min^{-1}$ on a Dupont 1090 thermal analyzer. The concentration of $Zn^{2+}$ in the solution of ZnO and the $C_3N_4$/ZnO photocatalytic system was measured as follows: at certain time intervals, 10 mL aliquots were sampled and centrifuged 5 times to remove all the particles. The filtrates were determined on a ThermoFisher IRIS Intrepid II XSP ICP-OES instrument. The total organic carbon (TOC) was measured with a Tekmar Dohrmann Apollo 9000 TOC analyzer. The photocurrents were measured on an electrochemical system (CHI-660B, China). UV light was obtained from an 11 W germicidal lamp and visible irradiation was obtained from a 500 W xenon lamp (Institute for Electric Light Sources, Beijing) with a 450 nm cutoff filter. A standard three-electrode cell with a working electrode (as-prepared photocatalyst), a platinum wire as counter electrode, and a standard calomel electrode (SCE) as reference electrode were used in the photoelectric studies. 0.1 M $Na_2SO_4$ was used as the electrolyte solution. Potentials are given with reference to the SCE. The photoresponses of the photocatalysts as light on and off were measured at 0.0 V.

### Photocatalytic experiments

The photocatalytic activities were evaluated by the decomposition of MB under UV light (λ = 254 nm) and visible light irradiation. The radial flux was measured by a power meter from the Institute of Electric Light Sources, Beijing. UV light was provided by an 11 W UV-light lamp (Institute of Electric Light Sources, Beijing) and the average light intensity was 0.8 mW $cm^{-2}$. An aqueous solution of MB (100 mL, 10 mg $L^{-1}$) was placed in a vessel, and 50 mg photocatalyst was added. Prior to irradiation, the suspensions were magnetically stirred in the dark for about 30 min. At certain time intervals, 2 mL aliquots were sampled and centrifuged to remove the particles. The filtrates were analyzed by recording variations of the maximum

absorption peak (663 nm for MB) using a Hitachi U-3010 UV-vis spectrophotometer. To estimate the photostability of the photocatalysts, 96 h persistent MB degradation of ZnO and $C_3N_4$/ZnO-2% were performed. At certain time intervals (24 h, 48 h and 96 h), the MB degradation performance of ZnO and $C_3N_4$/ZnO-2% was determined. The visible light was obtained by a halogen-tungsten lamp (provides visible light in the range of 400–800 nm; the main wavelength is about 550 nm) and the average visible light intensity was 1.2 mW $cm^{-2}$. The method was similar with the UV light degradation. The active species generated in the photocatalytic system could be detected through trapping by *tert*-butyl alcohol (*t*-BuOH) and ethylenediaminetetraacetic acid disodium salt (EDTA-2Na).

## Results and discussion

### Enhancement of photocatalytic activity and photocurrent

Fig. 1 shows the photocatalytic activity of ZnO and the $C_3N_4$/ZnO photocatalysts with different loading amounts of $C_3N_4$ under UV light and visible light irradiation, respectively. The mechanically blended $C_3N_4$ and ZnO (3%) were used as a reference. The photocatalytic degradation process was fitted to pseudo-first-order kinetics, and the value of the rate constant *k* is equal to the corresponding slope of the fitting line. As can be seen in Fig. 1A, the photocatalytic activity of the blended $C_3N_4$ and ZnO sample was almost the same as that of the pure ZnO, whereas all of the $C_3N_4$/ZnO photocatalysts exhibited higher photocatalytic activity than the pure ZnO sample under UV light irradiation. The photocatalytic activity was enhanced gradually with the increasing proportion of $C_3N_4$. When the proportion of $C_3N_4$ reached 3%, the as-prepared photocatalyst exhibited the highest photocatalytic activity. The apparent rate constant *k* was 0.0379 $min^{-1}$ and was almost 3.5 times as high as that of pure ZnO. However, further increasing the proportion of $C_3N_4$, the degradation rate decreased gradually though it remained higher than that of ZnO. It can also be seen from the insert graph of Fig. 1A that the loading amount of $C_3N_4$ had a great influence on the photocatalytic activity of the as-prepared photocatalysts. The optimal loading amount of $C_3N_4$ on the surface of ZnO was 3%. To further understand the mineralization property of the as-prepared photocatalyst, the decrease of TOC in the photodegradation of MB by ZnO and $C_3N_4$/ZnO-3% photocatalysts was determined (see supplementary data Figure S1†). It was found that the TOC removal percentage is 64% and 32% for $C_3N_4$/ZnO-3% and ZnO after 2 h photocatalytic reaction, respectively. After $C_3N_4$ modification, the mineralization property of ZnO was evidently enhanced. Under visible light irradiation, since ZnO could not be excited by visible light irradiation, the pure ZnO played no role in degrading MB. After modification with $C_3N_4$, ZnO possessed excellent visible light photocatalytic activity (see Fig. 1B), and the photocatalytic activity is much higher than that of pure $C_3N_4$. The $C_3N_4$/ZnO-3% photocatalyst could degrade MB by 72.3% in 5 h. It was notable that the mechanical blend did not obviously enhance the photocatalytic activity of ZnO, implying that there may be some interaction between ZnO and $C_3N_4$ that plays an important role in improving the photocatalytic activity.

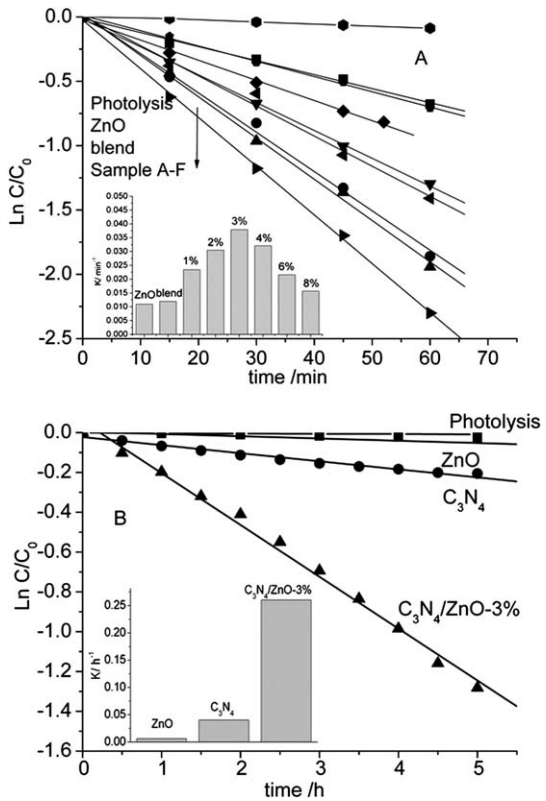


**Fig. 1** Photolysis of MB and photocatalytic degradation of MB over ZnO and $C_3N_4$/ZnO photocatalysts (A) under UV light irradiation ($\lambda = 254$ nm) and (B) under visible light irradiation (visible light region in the range of 400–800 nm; the main wavelength is about 550 nm); MB initial concentration = 10 mg $L^{-1}$. Samples A–F represent $C_3N_4$/ZnO photocatalysts with 8%, 6%, 1%, 4%, 2%, and 3% of $C_3N_4$ loaded, respectively. Inserts: degradation rate constant *k* of ZnO, $C_3N_4$ and various $C_3N_4$/ZnO photocatalysts.

Photocurrents were measured for $C_3N_4$/ZnO-3% and ZnO electrodes to investigate the electronic interaction between $C_3N_4$ and ZnO (Fig. 2). It was clear that fast and uniform photocurrent responses were observed in both electrodes and the photoresponsive phenomenon was entirely reversible. Under UV light irradiation, the photocurrent of the $C_3N_4$/ZnO-3% electrode was about five times as high as that of the pure ZnO electrode (Fig. 2A). Under visible light irradiation, ZnO showed almost no photocurrent response. On the contrary, $C_3N_4$/ZnO-3% photocatalyst showed a noticeable photocurrent under visible light irradiation (Fig. 2B). The photocurrent enhancement of the $C_3N_4$/ZnO photocatalyst indicated an enhanced photoinduced electrons and holes separation, which could be attributed to the synergetic effect of $C_3N_4$ and the ZnO semiconductor.

### Photocorrosion suppression

To estimate the photostability of the photocatalysts, 96 h persistent MB degradation of ZnO and $C_3N_4$/ZnO-2% was performed, and the rate constant *k* at a certain reaction time is shown in Fig. 3. Under UV light irradiation, 72% of MB could be degraded in 2 h when ZnO was used for the first time. After 24 h of photocatalytic reaction, a sharp decrease of photocatalytic activity of pure ZnO can be seen from Fig. 3 and the reaction rate constant *k* decreased from 0.0107 $min^{-1}$ to 0.0052 $min^{-1}$. After

 

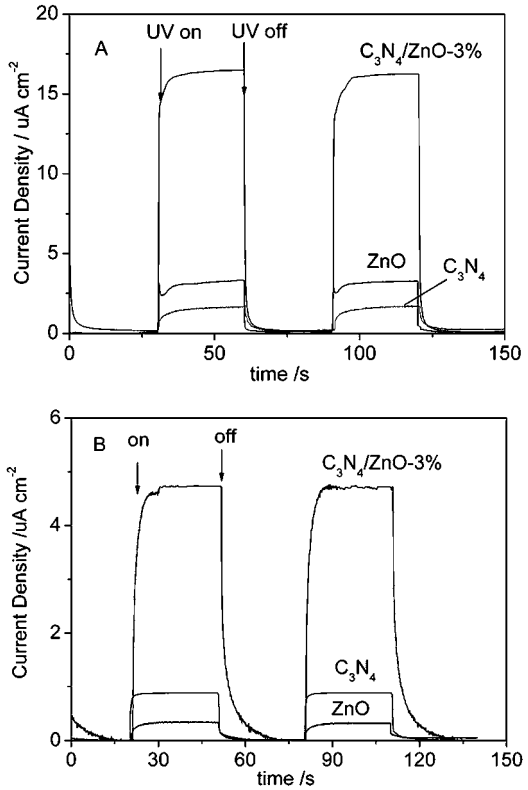


**Fig. 2** Photocurrents of ZnO, $C_3N_4$ and $C_3N_4$/ZnO electrodes (A) under UV light irradiation ($\lambda = 254$ nm) and (B) under visible light irradiation ($\lambda > 450$ nm) ([$Na_2SO_4$] = 0.1 M).

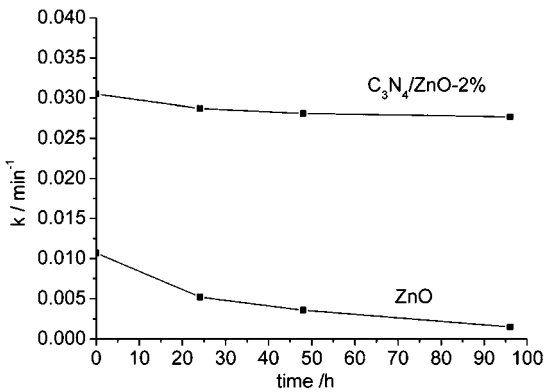


**Fig. 3** Photostability experiments of ZnO and $C_3N_4$/ZnO photocatalysts. (UV light $\lambda = 254$ nm, average light intensity = 0.8 mW cm$^{-2}$).

96 h of photocatalytic reaction, the photocorrosion of ZnO was very severe. The photocatalytic degradation of MB was hardly evident, and the reaction rate constant $k$ declined to 0.0015 min$^{-1}$, which was only one-seventh of the initial reaction rate (0.0107 min$^{-1}$). Interestingly, after hybridization with $C_3N_4$, long time photocatalytic reaction did not conspicuously affect the photocatalytic activity of ZnO. The reaction rate constant $k$ decreased from 0.0305 min$^{-1}$ to 0.0277 min$^{-1}$ after 96 h photodegradation, which still preserved 91% of the initial photocatalytic activity. Apparently, the presence of $C_3N_4$ on the surface of ZnO could inhibit the photocorrosion phenomenon and enhance the stability of the ZnO photocatalyst greatly.

To further investigate the suppression of photocorrosion, XRD patterns, TEM images and ICP-OES were determined before and after photocatalytic reaction. Figure S2 shows the XRD patterns of ZnO and $C_3N_4$/ZnO-2% before and after 48 h photocatalytic reaction.† For pure ZnO, after 48 h photocatalytic reaction, new diffraction peaks appeared at 27.7°, 32.8°, and 60.1°, which could be attributed to the $Zn_5(OH)_6(CO_3)_2$ phase. The crystalline phase structure of ZnO was obviously destroyed, indicating that severe photocorrosion had taken place. However, the XRD patterns of $C_3N_4$/ZnO-2% showed no notable differences before and after 48 h photocatalytic reaction. The TEM images of ZnO and $C_3N_4$/ZnO-2% photocatalysts before and after 48 h reaction are shown in Figure S3.† Before reaction, the ZnO and $C_3N_4$/ZnO-2% samples consisted of agglomerated approximately spherical particles with diameters of 20 nm. After 48 h photocatalytic reaction, for pure ZnO, only loose floccule existed, indicating that the structure of the ZnO crystal had been serious destroyed. In contrast, for the $C_3N_4$/ZnO-2% sample before and after 48 h photocatalytic reaction, it had not exhibited any great changes in morphology, revealing that $C_3N_4$-hybridized ZnO was photostable and the photocorrosion was successfully suppressed.

The concentrations of $Zn^{2+}$ in the solution of ZnO and the $C_3N_4$/ZnO-2% photocatalytic system before and after photocatalytic reaction are shown in Table 1. After 4 h of reaction, the concentration of $Zn^{2+}$ was 9.485 μg mL$^{-1}$ and 7.264 μg mL$^{-1}$ in ZnO and $C_3N_4$/ZnO-2% photocatalytic solution, respectively. After 24 h of photocatalytic reaction, the concentration of $Zn^{2+}$ was 389.500 μg mL$^{-1}$ in the solution of the ZnO photocatalytic system, indicating that the structure of ZnO was destroyed and a large amount of ZnO particles was dissolved in the solution. Interestingly, after 24 h of photocatalytic reaction, the concentration of $Zn^{2+}$ was 8.078 μg mL$^{-1}$ in the solution of $C_3N_4$/ZnO-2% photocatalytic system which was not evidently different from that after 4 h reaction. The ICP results were in good agreement with the results of TEM and XRD, further revealing that the presence of $C_3N_4$ on the ZnO surface could effectively suppress the photocorrosion of ZnO during the photocatalytic reaction.

### Structure and morphology of $C_3N_4$/ZnO photocatalysts

Fig. 4 shows an HRTEM image of $C_3N_4$/ZnO-3% photocatalyst. As can be seen from Fig. 4, the lattice structure of ZnO was very orderly and the outer boundary of the as-prepared sample was distinctly different from the ZnO core. The measured interplanar spacing is 0.136 nm which corresponds to the ZnO (201) plane. The thickness of the $C_3N_4$ layer coated on the $C_3N_4$/ZnO-3% sample was about 0.354 nm, which is close to the scale of

**Table 1** The concentrations of $Zn^{2+}$ in the solutions of ZnO and the $C_3N_4$/ZnO-2% photocatalytic system before and after different times of photocatalytic reaction

| Photocatalyst | Before reaction (μg mL$^{-1}$) | After 4 h reaction (μg mL$^{-1}$) | After 24 h reaction (μg mL$^{-1}$) |
|---|---|---|---|
| ZnO | 1.940 | 9.485 | 389.500 |
| $C_3N_4$/ZnO-2% | 1.247 | 7.264 | 8.078 |

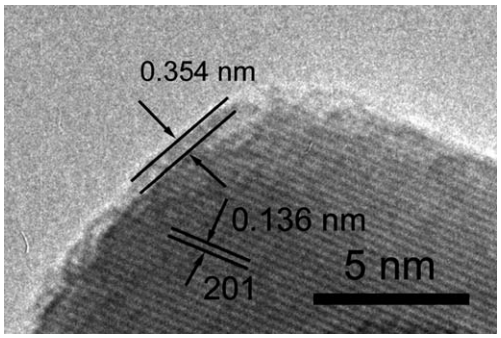


**Fig. 4** HRTEM image of $C_3N_4$/ZnO-3% photocatalyst.



monolayer $C_3N_4$ (about 0.325 nm).[32] Therefore, it can be inferred that the $C_3N_4$ molecule was dispersed on the surface of ZnO with an approximately monolayer structure.

The amount of $C_3N_4$ could be obtained by TG analysis (Figure S4†). For pure ZnO, a weight loss occurring from 200 °C to 500 °C could be attributed to the desorption of surface bound water. For pure $C_3N_4$, two weight loss regions could be seen in the TG curve. The first weight loss could also be attributed to the desorption of surface bound water. The second weight loss occurring from 500 °C to 720 °C could be assigned to the burning of $C_3N_4$. These two weight loss regions could be seen in all $C_3N_4$/ZnO samples. The amount of $C_3N_4$ hybridized on the surface of ZnO could be calculated from the second weight loss and is shown in the insert of Figure S4.† Except for the $C_3N_4$/ZnO-8% sample, the amount of $C_3N_4$ was nearly consistent to the dosage of $C_3N_4$ added.

The XRD patterns of ZnO, $C_3N_4$ and various $C_3N_4$/ZnO photocatalysts are shown in Fig. 5. As can be seen from Fig. 5 the crystal phase of ZnO did not change after hybridization. All the diffraction peaks of the ZnO can be exactly indexed as the zincite structure (JCPDS 89-1397). There was no crystalline $C_3N_4$ in the $C_3N_4$/ZnO photocatalysts with low $C_3N_4$ loadings, whereas the as-prepared samples with higher $C_3N_4$ loadings (>3%) exhibited a crystalline $C_3N_4$ peak; the peak intensities increased with the increase in $C_3N_4$ loading. Thus, it can be inferred that $C_3N_4$ was dispersed uniformly on the ZnO surface with low $C_3N_4$ loadings,[33] while crystalline $C_3N_4$ appeared only if its loading exceeded a threshold value (3%).

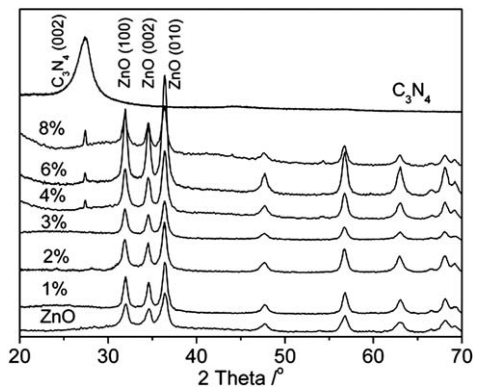


**Fig. 5** XRD of ZnO, $C_3N_4$ and $C_3N_4$/ZnO photocatalysts.

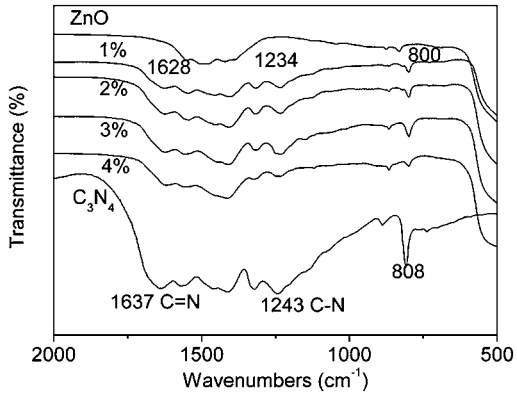


**Fig. 6** FT-IR spectra of ZnO, $C_3N_4$ and $C_3N_4$/ZnO photocatalysts.

Fig. 6 shows the FT-IR spectra of ZnO and various $C_3N_4$/ZnO photocatalysts. In the FT-IR spectrum of $C_3N_4$, the peaks at 1637 $cm^{-1}$ and 1243 $cm^{-1}$ were attributable to the C=N and C–N stretching vibration modes, respectively.[34,35] The peak at 808 $cm^{-1}$ was related to the s-triazine ring modes.[35] It can be clearly seen that the main characteristic peaks of $C_3N_4$ and ZnO all appeared in the $C_3N_4$/ZnO photocatalysts. In the $C_3N_4$/ZnO photocatalysts, all of the main characteristic peaks of $C_3N_4$ moved to a lower wavenumber. The red shift of these bands indicated that the bond strengths of C–N and C=N were weakened, suggesting that the conjugated system of $C_3N_4$ was stretched and a more widely conjugated system containing $C_3N_4$ and ZnO had already appeared. The FT-IR spectra revealed the existence of $C_3N_4$ structure and there was a covalent bond between $C_3N_4$ and ZnO.[21] This bond may be of significance to transfer carriers and induce a synergetic effect to enhance the photocatalytic activity. The Raman spectra can not be obtained due to the fluorescence of $C_3N_4$.

The UV-vis DRS spectra of ZnO and different mass ratios of $C_3N_4$/ZnO photocatalysts are shown in Fig. 7. As expected, a sharp fundamental absorption edge rises at 410 nm for ZnO. Compared with that of pure ZnO, the $C_3N_4$/ZnO photocatalysts show the same absorbance edge, but extend the absorbance to the visible region due to the presence of $C_3N_4$ on the ZnO surface. The absorption edge does not shift for all $C_3N_4$/ZnO samples, indicating identical band gap energies. The absorption intensity of the prepared samples increases with increasing amounts of $C_3N_4$.

### Mechanism of enhancement of photoactivity and photocorrosion suppression under UV irradiation

It is well known that the photocatalytic activity is mainly governed by phase structure, adsorption ability, and separation efficiency of photogenerated electrons and holes.[36,37] As can be seen from the XRD spectra, the crystal phase structure of ZnO was not changed during the hybridization. An adsorption experiment was performed to evaluate the adsorption ability of the ZnO and $C_3N_4$/ZnO photocatalysts in the dark (see Figure S5†). As can be seen from Figure S5,† after equilibration in the dark for 10 min, 89.2% and 74.9% of MB remained in the solution with pure ZnO and $C_3N_4$/ZnO-3% photocatalyst, respectively. However, there were no significant changes in the BET surface area (37.741 and 37.832 $m^2$ $g^{-1}$ for ZnO and

 

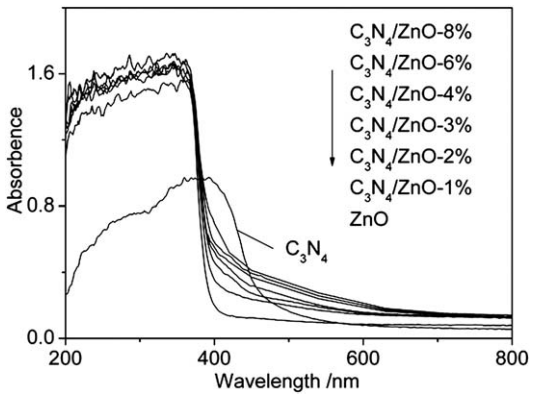


**Fig. 7** UV-vis DRS of $C_3N_4$, ZnO and $C_3N_4$/ZnO photocatalysts.

$C_3N_4$/ZnO-3%, respectively) between ZnO and $C_3N_4$/ZnO-3%, indicating the MB adsorption should not just originate from simply physical adsorption. The enhancement of adsorption could be contributed to the π–π stacking between MB and $C_3N_4$, which was similar to the conjugation between aromatic molecules and graphene.[36] MB molecules could be adsorbed on the $C_3N_4$ surface with offset face to face orientation *via* π–π conjugation until an adsorption–desorption equilibrium is reached. The enhanced adsorptivity was a good supplement for the high photocatalytic activity of the hybridized $C_3N_4$/ZnO photocatalyst.

It is important to detect the main oxidative species in the photocatalytic process for revealing the photocatalytic mechanism. The main oxidative species in the photocatalytic process could be detected through the trapping experiments of radicals and holes by using *t*-BuOH (radical scavenger)[38] and EDTA-2Na (hole scavenger),[39] respectively. As shown in Fig. 8A, in the ZnO system, the addition of a scavenger of radicals (*t*-BuOH) only caused a small change in the photodegradation of MB. On the contrary, the photocatalytic activity of ZnO could be greatly suppressed by the addition of a scavenger for holes (EDTA-2Na). This result suggested that the photogenerated holes were the main oxidative species of the ZnO system. In the $C_3N_4$/ZnO system (see Fig. 8B), the photocatalytic activity was greatly prevented by the EDTA-2Na, indicating the main oxidative species is the same as that of ZnO.

As discussed above, the crystal phase structure and surface area was not evidently changed and the limited adsorptivity enhancement was not the major factor of the significant enhancement of the photocatalytic activity of ZnO (enhanced about 3.5 times). The significant enhancement of photocatalytic activity was mainly due to the high efficiency of charge separation induced by the hybrid effect of $C_3N_4$ and ZnO. A schematic for electron–hole separation and transportation at the $C_3N_4$/ZnO photocatalyst interface is shown in Fig. 9. ZnO can be excited by UV light and produce photogenerated electron–hole pairs, showing photocatalytic activity. Since the valence band (VB) position of ZnO is lower than the highest occupied molecular orbital (HOMO) of $C_3N_4$,[32,40] the photogenerated holes on ZnO could directly transfer to $C_3N_4$, making charge separation more efficient and reducing the probability of photogenerated electron–hole recombination, leading to an enhanced photocatalytic activity.

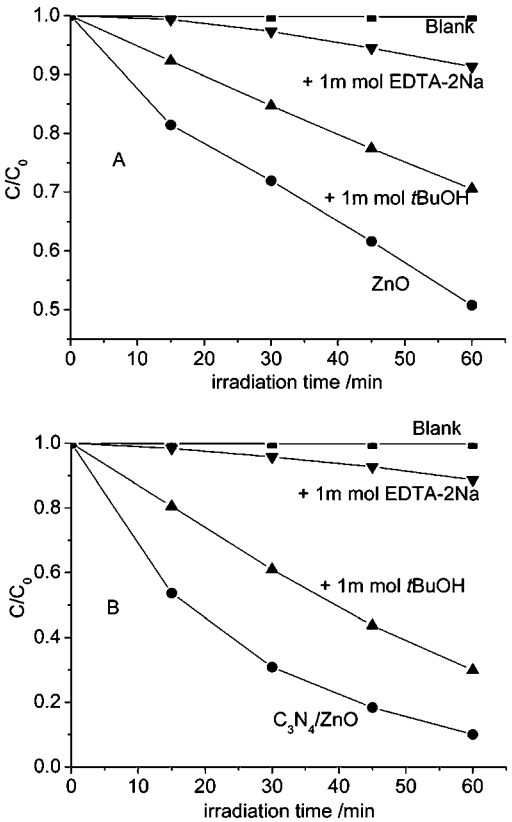


**Fig. 8** The plots of photogenerated carriers trapping in the system of photodegradation of MB by (A) ZnO and (B) $C_3N_4$/ZnO under UV light irradiation.

As shown above, beyond the higher photocatalytic activity, the presence of $C_3N_4$ could effectively enhance the photostability of ZnO photocatalyst. Many reports have suggested that ZnO semiconductor suffers from a significant decrease in photocatalytic activity due to the photoinduced dissolution.[20] The photocorrosion process of ZnO can be presented as follows:

$$ZnO + 2h^+ + nH_2O \rightarrow Zn(OH)_n^{(2-n)+} + \frac{1}{2}O_2 + nH^+ \qquad (1)$$

where *n* depends on the pH of the solution.[20] As can be seen from eqn (1), the photoinduced holes participate in the photocorrosion

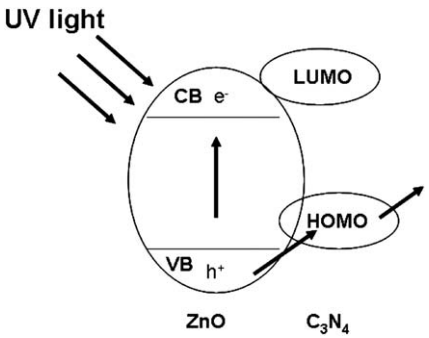


**Fig. 9** Schematic drawing illustrating the mechanism of charge separation and photocatalytic activity of the $C_3N_4$/ZnO photocatalyst under UV light irradiation.

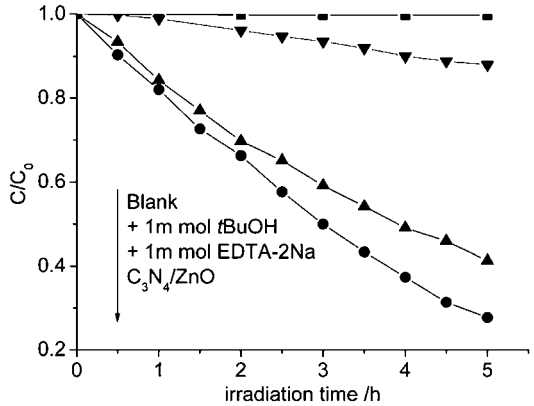


**Fig. 10** The plots of photogenerated carriers trapping in the system of photodegradation of MB by $C_3N_4$/ZnO-3% under visible light irradiation.

and destroy the crystal structure of ZnO. As a result, the photocatalytic activity of ZnO is greatly decreased. After introduction of $C_3N_4$ to ZnO, the photogenerated holes on ZnO could transfer to $C_3N_4$, and then effective photocorrosion inhibition is achieved.

### Mechanism of visible photoactivity

As it is well known that ZnO itself can not be excited by visible light, the trapping experiments of radicals and holes were only performed on $C_3N_4$/ZnO-3% photocatalyst. As can be seen from Fig. 10, the photodegradation of MB was obviously suppressed after the injection of *t*-BuOH. This result suggests that radicals are the main oxidative species in this system. On the basis of the results of photodegradation and photogenerated carrier trapping test, a proposed schematic mechanism of the visible light activity of the $C_3N_4$/ZnO photocatalyst is shown in Fig. 11. $C_3N_4$ absorbs visible light to induce $\pi$–$\pi^*$ transition, transporting the excited-state electrons from the HOMO to the lowest unoccupied molecular orbital (LUMO). The LUMO potential of $C_3N_4$ (−1.12 eV)[32] is more negative than the conduction band (CB) edge of ZnO (−0.5 eV),[20] so the excited electron on $C_3N_4$ could directly inject into the CB of ZnO. $C_3N_4^+$ would accept electrons from fragments of MB degradation and return to the ground state. The electrons would subsequently transfer to the photocatalyst surface to react with water and oxygen to generate superoxide and hydroxyl radicals. The radicals are able to oxidize the pollutant due to their high oxidative capacity, producing visible light photocatalytic activity.

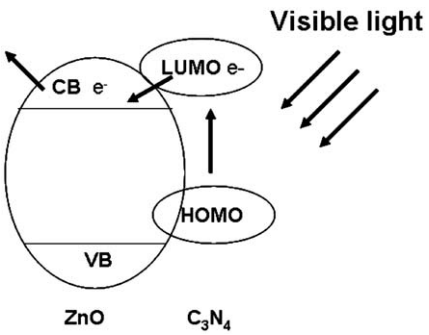


**Fig. 11** Schematic drawing illustrating the mechanism of charge separation and photocatalytic activity of the $C_3N_4$/ZnO photocatalyst under visible light irradiation.

## Conclusion

A $C_3N_4$/ZnO photocatalyst was successfully synthesized *via* a facile chemisorption. After introduction of $C_3N_4$, the photocurrent of ZnO was enhanced by 5 times under UV light irradiation and a noticeable photocurrent was observed under visible light irradiation. The $C_3N_4$/ZnO photocatalyst possessed significantly enhanced UV light photocatalytic activity, visible light photocatalytic activity and excellent antiphotocorrosion ability. The performance enhancement and photocorrosion inhibition under UV light irradiation were induced by the high separation efficiency of photoinduced charges. The visible photoactivity originated from the injection of excited electrons from the LUMO of $C_3N_4$ to the CB of ZnO. $C_3N_4$ hybridization is demonstrated to be a promising approach to design highly active and stable ZnO photocatalysts.

## Acknowledgements

This work was partly supported by Chinese National Science Foundation (20925725 and 20673065) and National Basic Research Program of China (2007CB613303).

## References

1 A. Mills and S. Le Hunte, *J. Photochem. Photobiol., A*, 1997, **108**, 1–35.
2 A. L. Linsebigler, G. Lu and J. T. Yates, *Chem. Rev.*, 1995, **95**, 735–758.
3 B. Dindar and S. Icli, *J. Photochem. Photobiol., A*, 2001, **140**, 263–268.
4 M. Cristina Yeber, J. Rodranuez, J. Freer, N. Duron and H. D. Mansilla, *Chemosphere*, 2000, **41**, 1193–1197.
5 A. A. Khodja, T. Sehili, J.-F. Pilichowski and P. Boule, *J. Photochem. Photobiol., A*, 2001, **141**, 231–239.
6 C. Ye, Y. Bando, G. Shen and D. Golberg, *J. Phys. Chem. B*, 2006, **110**, 15146–15151.
7 B. Cao and W. Cai, *J. Phys. Chem. C*, 2007, **112**, 680–685.
8 X. Qiu, L. Li, J. Zheng, J. Liu, X. Sun and G. Li, *J. Phys. Chem. C*, 2008, **112**, 12242–12248.
9 X. Q. Qiu, G. S. Li, X. F. Sun, L. P. Li and X. Z. Fu, *Nanotechnology*, 2008, **19**, 1–8.
10 J. Bandara, K. Tennakone and P. P. B. Jayatilaka, *Chemosphere*, 2002, **49**, 439–445.
11 J. Liqiang, W. Baiqi, X. Baifu, L. Shudan, S. Keying, C. Weimin and F. Honggang, *J. Solid State Chem.*, 2004, **177**, 4221–4227.
12 A. L. S. Stroyuk, V. V. Kuchmii and S. Ya, *Theor. Exp. Chem.*, 2004, **40**, 98–104.
13 M. Zhang, T. An, X. Hu, C. Wang, G. Sheng and J. Fu, *Appl. Catal., A*, 2004, **260**, 215–222.
14 R. S. Mane, W. J. Lee, H. M. Pathan and S.-H. Han, *J. Phys. Chem. B*, 2005, **109**, 24254–24259.
15 X. G. Chen, Y. Q. He, Q. Zhang, L. J. Li and D. H. Hu, *J. Mater. Sci.*, 2010, **45**, 953–960.
16 R. Comparelli, E. Fanizza, M. L. Curri, P. D. Cozzoli, G. Mascolo and A. Agostiano, *Appl. Catal., B*, 2005, **60**, 1–11.
17 G. Yu, J. Gao, J. C. Hummelen, F. Wudl and A. J. Heeger, *Science*, 1995, **270**, 1789–1791.
18 L. Zhao, X. Chen, X. Wang, Y. Zhang, W. Wei, Y. Sun, M. Antonietti and M.-M. Titirici, *Adv. Mater.*, 2010, **22**, 3317–3321.
19 W. J. D. Beenken, *Chem. Phys.*, 2009, **357**, 144–150.
20 H. Fu, T. Xu, S. Zhu and Y. Zhu, *Environ. Sci. Technol.*, 2008, **42**, 8064–8069.



 

21 H. Zhang, R. Zong and Y. Zhu, *J. Phys. Chem. C*, 2009, **113**, 4605–4611.
22 L. Zhang, H. Cheng, R. Zong and Y. Zhu, *J. Phys. Chem. C*, 2009, **113**, 2368–2374.
23 A. Thomas, A. Fischer, F. Goettmann, M. Antonietti, J.-O. Muller, R. Schlogl and J. M. Carlsson, *J. Mater. Chem.*, 2008, **18**, 4893–4908.
24 J. M. Hu, *Appl. Phys. Lett.*, 2006, **89**, 261117.
25 X. Wang, K. Maeda, A. Thomas, K. Takanabe, G. Xin, J. M. Carlsson, K. Domen and M. Antonietti, *Nat. Mater.*, 2009, **8**, 76–80.
26 K. Takanabe, K. Kamata, X. Wang, M. Antonietti, J. Kubota and K. Domen, *Phys. Chem. Chem. Phys.*, 2010, **12**, 13020–13025.
27 K. Maeda, X. Wang, Y. Nishihara, D. Lu, M. Antonietti and K. Domen, *J. Phys. Chem. C*, 2009, **113**, 4940–4947.
28 X. Wang, K. Maeda, X. Chen, K. Takanabe, K. Domen, Y. Hou, X. Fu and M. Antonietti, *J. Am. Chem. Soc.*, 2009, **131**, 1680–1681.
29 Z. Ding, X. Chen, M. Antonietti and X. Wang, *ChemSusChem*, 2011, **4**, 274–281.
30 Y. Di, X. Wang, A. Thomas and M. Antonietti, *ChemCatChem*, 2010, **2**, 834–838.
31 S. C. Yan, Z. S. Li and Z. G. Zou, *Langmuir*, 2010, **26**, 3894–3901.
32 S. C. Yan, S. B. Lv, Z. S. Li and Z. G. Zou, *Dalton Trans.*, 2010, **39**, 1488–1491.
33 L. Lin, W. Lin, Y. X. Zhu, B. Y. Zhao, Y. C. Xie, G. Q. Jia and C. Li, *Langmuir*, 2005, **21**, 5040–5046.
34 Y. Zhao, D. Yu, H. Zhou, Y. Tian and O. Yanagisawa, *J. Mater. Sci.*, 2005, **40**, 2645–2647.
35 X. Li, J. Zhang, L. Shen, Y. Ma, W. Lei, Q. Cui and G. Zou, *Appl. Phys. A: Mater. Sci. Process.*, 2009, **94**, 387–392.
36 H. Zhang, X. Lv, Y. Li, Y. Wang and J. Li, *ACS Nano*, 2009, **4**, 380–386.
37 L. W. Zhang, H. B. Fu and Y. F. Zhu, *Adv. Funct. Mater.*, 2008, **18**, 2180–2189.
38 H. Lee and W. Choi, *Environ. Sci. Technol.*, 2002, **36**, 3872–3878.
39 J. Zhou, C. Deng, S. Si, Y. Shi and X. Zhao, *Electrochim. Acta*, 2011, **56**, 2062–2067.
40 A. Hagfeldt and M. Graetzel, *Chem. Rev.*, 1995, **95**, 49–68.